ACS Energy LETTERS

http://pubs.acs.org/journal/aelccp

Deciphering the Impact of the Active Lithium Reservoir in Anode-Free Pouch Cells

Charlotte Gervillié-Mouravieff, Louis Ah, Alex Liu, Chen-Jui Huang, and Ying Shirley Meng*

Cite This: *ACS Energy Lett.* 2024, 9, 1693−1700

Read Online

ACCESS | Metrics & More | Article Recommendations | Supporting Information

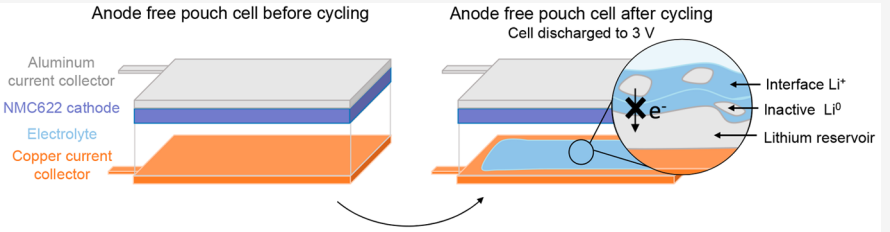

ABSTRACT: **Anode-free batteries, which revolutionize energy storage by discarding traditional anodes in favor of copper foil to plate lithium directly from the cathode, offer increased energy densities and better safety than conventional lithium metal cells. However, their advantage is tempered by a significantly reduced cycle life, attributed to lithium loss through parasitic reactions. Comprehending the lithium inventory evolution under diverse conditions is vital for developing strategies to improve their performance. Herein, using coulometry, titration gas chromatography, and cryogenic scanning electron microscopy, we analyze the evolution of active and inactive lithium in NMC622||Cu pouch cells. Our results reveal the mechanism of lithium reservoir formation due to cathode irreversibility and its subsequent impact on cell performance across various electrolytes. Our findings not only highlight the significance of the lithium reservoir for anode-free cells' cycle life but also explore its modulation through charge/discharge rates, offering new opportunities to understand and enhance anode-free cells' cycle life.**

Anode-free batteries are the ultimate choice for lithium metal batteries and represent an innovative paradigm in electrochemical energy storage. This configuration challenges traditional designs by eliminating conventional anodes and plating lithium directly from the cathode onto bare copper foil during charging. This design offers increased gravimetric and volumetric energy density, reduced cost, and utmost safety in the realm of lithium metal batteries.[1] However, the commercialization of anode-free batteries is significantly hindered by the formation of dendritic lithium during the charging process, leading to continuous parasitic reactions with the electrolyte and large volume changes.[2] As a result, inactive ("dead") lithium accumulates over cycling, including (electro)chemically formed Li^+ compounds in the solid electrolyte interphase (SEI) and isolated unreacted metallic Li^0, resulting in capacity loss and safety hazards. Additionally, these phenomena are accelerated in conventional carbonate-based electrolytes, where lithium tends to plate with a high-surface-area mossy morphology.[2,3] Nevertheless, recent advancements in electrolyte and current collector design have led to longer-lasting anode-free cells.[4−6] Notably, Ren et al. achieved 70 cycles with 80% capacity using a localized high-concentration electrolyte (LHCE),[7] with Niu et al. later confirming and enhancing these results, extending the cycle life to 100 cycles.[8] Yu et al. could maintain 80% capacity over 100 cycles with a single-solvent, single-salt electrolyte, and Louli et al. extended this to 200 cycles using a dual-salt carbonate-based electrolyte under optimal pressure and rate conditions.[9,10]

To continue enhancing the performance of anode-free cells, it appears crucial to differentiate and quantify the various forms of lithium in these cells and monitor their distribution and evolution throughout the cycling process, depending on various conditions such as pressure or electrolytes. Compared to lithium metal cells, the problem might appear simplified for anode-free cells, as there is no active lithium compensation from the anode, and all the active lithium is initially stored within the cathode. However, the intricate interplay of the cathode's first-cycle irreversibility and lithium plating/stripping efficiency significantly influences the shape of the capacity retention curves and the measurements of Coulombic

Received: February 12, 2024
Revised: March 18, 2024
Accepted: March 21, 2024

https://doi.org/10.1021/acsenergylett.4c00457
ACS Energy Lett. 2024, 9, 1693−1700

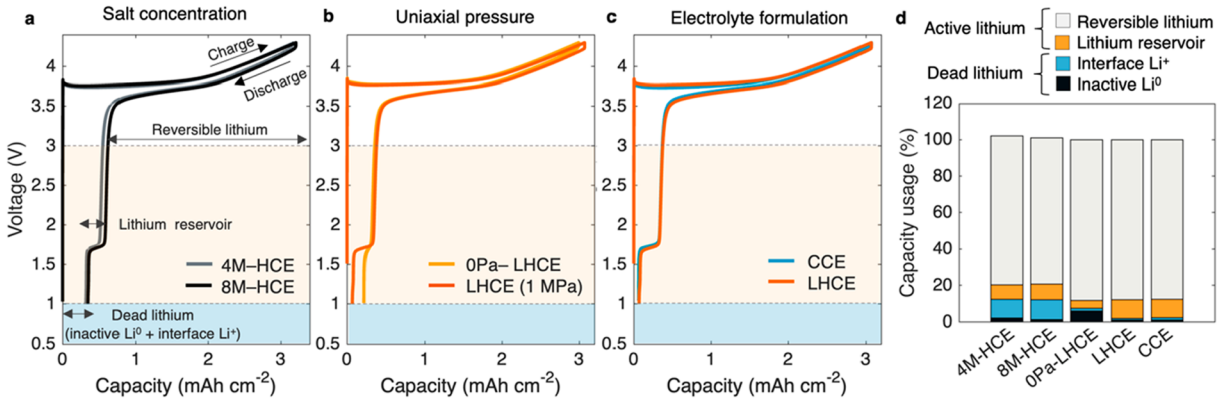

Figure 1. First cycle evolution of voltage vs capacity of anode-free NMC622||Cu pouch cells between 4.3 and 1 V at C/10-D/10 with (a) 4M-HCE and 8M-HCE, (b) LHCE (1 MPa) and 0Pa-LHCE, (c) LHCE and CCE. For indications, the salt concentration in LHCE and CCE is 1.7 and 1.2 M, respectively. (d) Lithium inventory at the anode for anode-free cells discharged to 3 V.

efficiency (CE). Interestingly, early work from Neudecker et al. reported that anode-free thin film could be transformed "in-situ" into lithium metal battery thanks to the $LiCoO_2$ cathode first cycle irreversibility.[11] Similarly, Genovese et al. demonstrated that for NMC532/Cu anode-free cells, the irreversibility of the cathode led to the formation of an active lithium reservoir at the anode.[12] Additionally, the group reported that the first cycle irreversibility could be recovered after a discharge at low potential, proving the presence of remaining active lithium at the anode.[13,14] Drawing inspiration from these pioneering works, it becomes apparent that, in addition to studying dead and active lithium evolution, the lithium reservoir remaining at the anode in anode-free cells requires investigation. Indeed, while a limited number of studies report the presence of this active lithium reservoir, none of them provide a qualitative and quantitative explanation of its impact on anode-free cell performance.

Herein we aim to clarify the contribution of the lithium reservoir to the anode-free cell performances. We report a systematic study of the active lithium reservoir and unreacted metallic Li^0 evolution in anode-free $LiNi_{0.6}Mn_{0.2}Co_{0.2}O_2$ (NMC622)||Copper (Cu) commercial pouch cells, utilizing coulometry and titration gas chromatography. By coupling the quantification techniques to observations of the anode local microstructure by cryogenic scanning electron microscopy, we elucidate the formation and evolution mechanisms of the lithium reservoir and inactive metallic lithium in different types of electrolytes. Lastly, we explore the potential tuning of the lithium reservoir through different charge/discharge ratios, with significant implications for the cycle life of anode-free cells.

To investigate the lithium inventory within anode-free pouch cells, NMC622||Cu cells were charged to 4.3 V and completely discharged to 1 V. As illustrated in Figure 1a–c, different electrolyte formulations were investigated: a high-concentration electrolyte (4M-HCE; LiFSI-2.4DME (molar) and 8M-HCE; LiFSI-1.2DME (molar)), a commercial carbonate-based electrolyte (CCE; 1.2 M $LiPF_6$ in EC/DEC + 10 wt % FEC), and a localized highly concentrated electrolyte (LHCE; LiFSI-1.2DME-3TTE (molar)). Interestingly, all the voltage curves, presented in Figure 1a–c, exhibit similar shapes with a reversible charge and discharge slope between 4.3 and 3 V and a short voltage plateau in discharge at 1.6 V. In layered oxide cathodes, 12–30% of the lithium extracted in the first charge cannot be reintercalated upon discharge due to very slow lithium kinetics as the lithium sites approach full occupancy.[15] However, residual active lithium stored at the anode can be recovered at low voltage through cathode overlithiation, leading to the formation of a Li_2NMC phase at 1.6 V.[16] This redox feature, observable on the derivative curves (see Supplementary Figure S1) is specific to nickel-based cathodes, as demonstrated in Supplementary Figure S1 by comparing the NMC622||Cu first cycle with $LiCoO_2$||Cu and $LiFePO_4$||Cu cells.

Consequently, capacity measurements conducted between 4.3 and 3 V and from 3 to 1 V were employed to evaluate reversible lithium intercalation in the cathode and the lithium reservoir, respectively. The remaining irreversibility at 1 V can then be attributed to dead lithium including the (electro)-chemically formed Li^+ compounds in the solid-electrolyte interface and cathode-electrolyte interface, referred to as SEI and CEI, respectively (interface Li^+), as well as electrically isolated unreacted metallic Li^0 (inactive Li^0).[2] Inactive Li^0 at the anode was quantified by titration gas chromatography (TGC),[17] and the lithium lost in interface Li^+ formation was calculated by subtracting the inactive Li^0 amount from the irreversibility at 1 V. Therefore, by utilizing the voltage curve from 4.3 to 1 V and TGC, the lithium inventory after one cycle can be calculated under various electrolytes and pressures, as summarized in Figure 1d.

We initially investigated the role of the salt concentration in the lithium inventory at the anode by comparing 4M-HCE to 8M-HCE under a uniaxial pressure of 1 MPa. Notably, in Figure 1a, the discharge capacity to 1 V is comparable for both cells, suggesting that salt concentration does not influence the active lithium inventory (comprising reversible lithium and the lithium reservoir). The slight change in the reversible lithium-to-lithium reservoir ratio can be attributed to the higher viscosity of 8M-HCE, which exacerbates the curve polarization. As a result, the 8M-HCE will reach the cutoff voltage of 3 V more quickly than the 4M-HCE. Additionally, both cells exhibit large irreversible Coulombic efficiency at 1 V, primarily attributed to the Li^+ interface, which is consistent with the known incompatibility of DME-based electrolytes with high-voltage cathodes (>4 V) due to poor oxidation stability.[18] Consequently, we turned to LHCE, a more representative electrolyte, to evaluate pressure's impact on lithium inventory.[7] In Figure 1b, voltage curves for cells with and without pressure

https://doi.org/10.1021/acsenergylett.4c00457
ACS Energy Lett. 2024, 9, 1693–1700

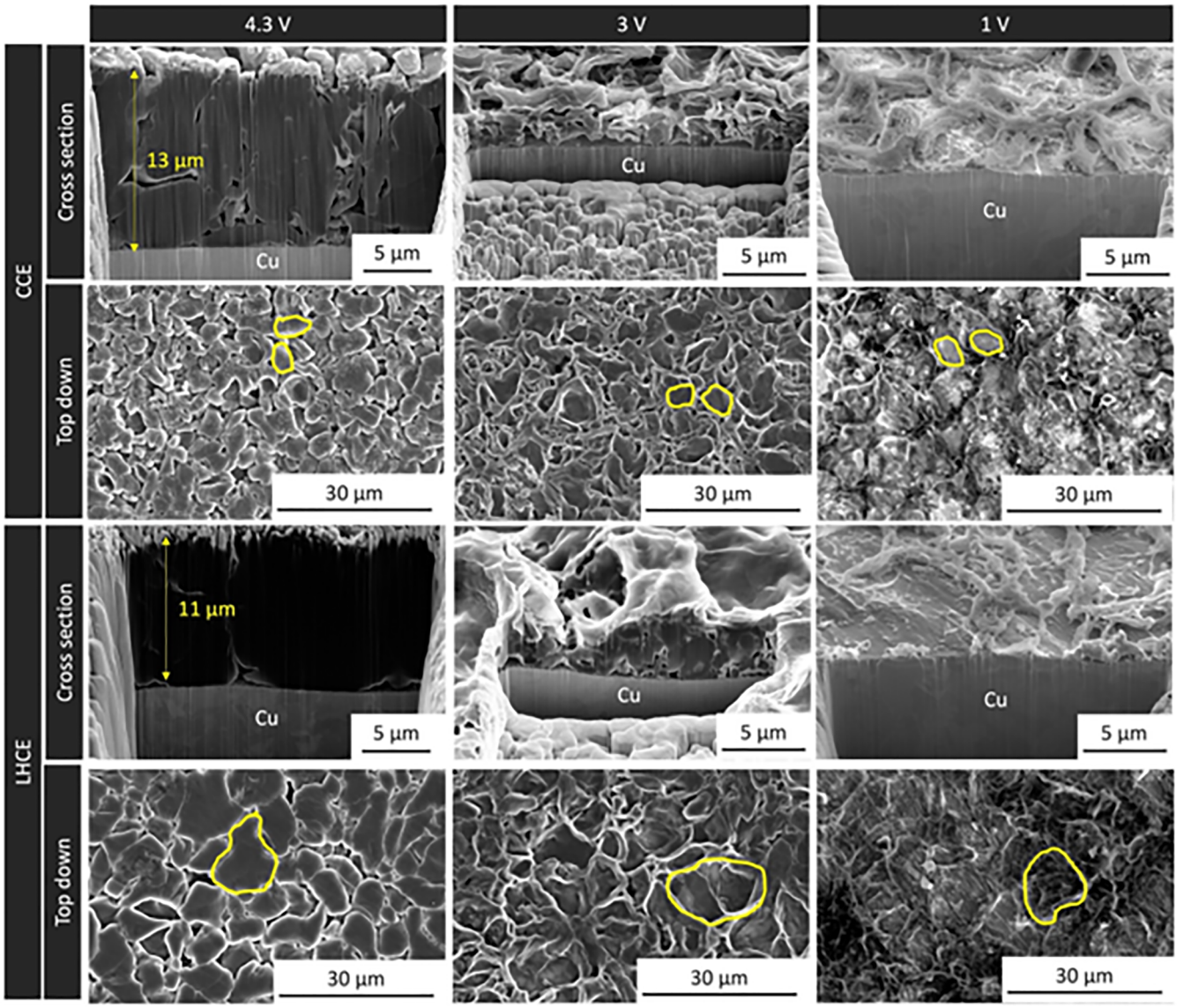

Figure 2. Cryo FIB-SEM images of the anode. Top-down and cross-sectional imaging of the copper current collector for anode-free cells cycled at 1 MPa with CCE and LHCE after charging to 4.3 V, discharging to 3 V, and fully discharging to 1 V.

overlap perfectly from 4.3 to 3 V. However, below 3 V, in the case of 0Pa-LHCE, the lithium reservoir has been nearly entirely depleted, transforming the active lithium into inactive Li^0, likely due to dendritic lithium morphology without pressure.[19] Lastly, LHCE was compared to CCE, with the latter electrolyte previously reported by Fang et al. as exhibiting the lowest first-cycle irreversibility among a wide array of electrolytes.[17] The two cells cycled at 1 MPa, demonstrate comparable voltage curves during the initial cycle (see Figure 1c), and discharging them to 1 V leads to a remarkable initial Coulombic efficiency (ICE) recovery of nearly 98%. The lithium inventory for anode-free cells using CCE and LHCE can then be described as follows: within the standard voltage range (4.3−3 V), after a single cycle, 88% of lithium is reversibly intercalated in the cathode, 10% remains active and formed a reservoir at the anode, 1% of inactive Li^0, and 1% of interfaces Li^+.

To reveal the morphology and formation mechanism of the lithium reservoir, cryogenic-focused ion beam−scanning electron microscopy (Cryo FIB−SEM) was employed, as illustrated in Figure 2. Strikingly, although the lithium inventory was comparable for cells cycled with CCE and LHCE, cross-sectional images after the initial charge to 4.3 V already reveal distinct differences between the two electrolyte types, with LHCE exhibiting denser plated lithium compared to CCE.[17,20] For the cells discharged to 3 V, the copper anode appears covered by an inhomogeneous layer of lithium, which is significantly denser with LHCE compared to CCE. The thickness of the active lithium reservoir at 3 V in LHCE and CCE cells is approximately 2 μm, which corresponds to 0.4 mAh cm^{-2} (assuming perfectly dense lithium). This value closely aligns with the quantification of the lithium reservoir by coulometry of 0.3 mAh cm^{-2} at 1.6 V, providing confirmation that the lithium observed at 3 V can be reintercalated into the cathode by discharging the cell to 1 V. Finally, for samples discharged to 1 V, only an extremely thin layer of lithium and interfacial components with a honeycomb-like morphology remains at the anode, confirming again the lithium inventory distribution proposed above. Note that this honeycomb-shaped layer accumulates over cycling to form a stack, while

https://doi.org/10.1021/acsenergylett.4c00457
ACS Energy Lett. 2024, 9, 1693−1700

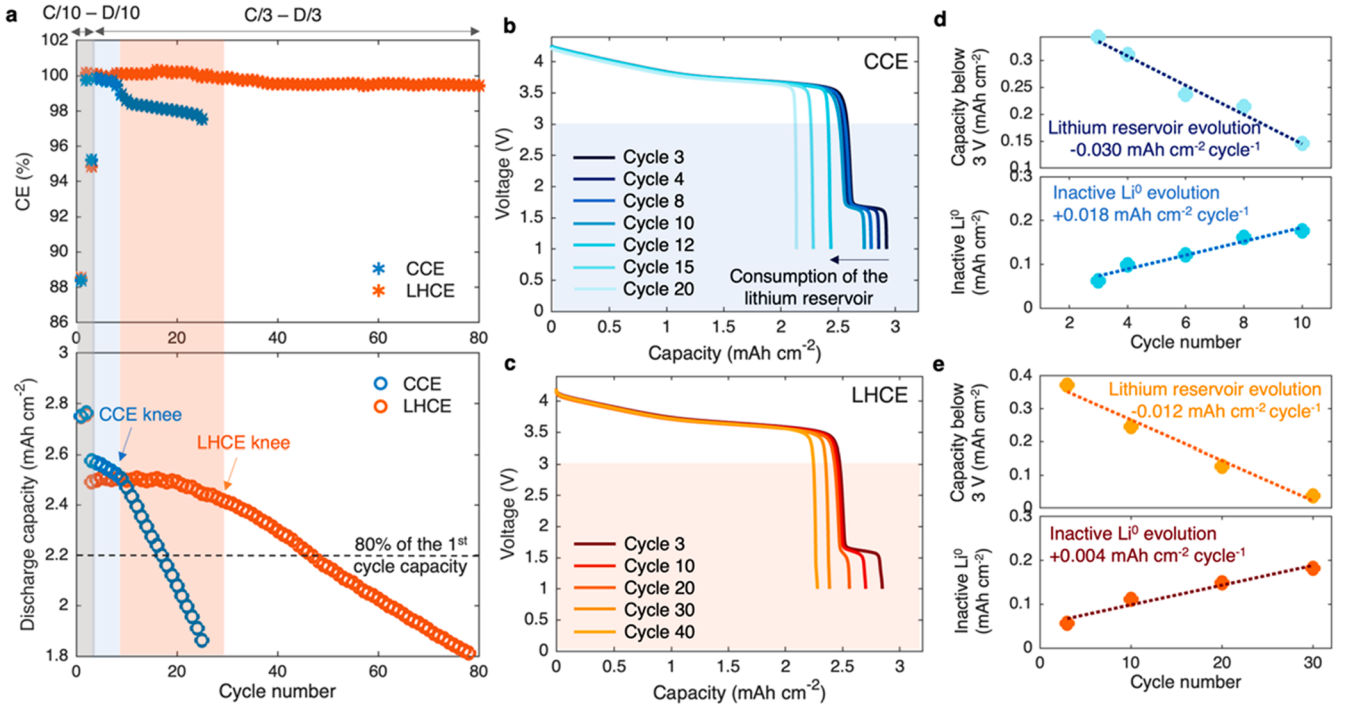

Figure 3. Lithium reservoir consumption and inactive Li^0 growth. After two cycles at C/10-D/10 between 4.3 and 3 V, the cells are then cycled at C/3-D/3 between 4.3 and 3 V. Only the last discharge is carried up to 1 V to evaluate the lithium reservoir evolution. (a) Coulombic efficiency and capacity retention of anode-free cells with CCE and LHCE electrolytes. (b, c) Discharged curves to 1 V evolution over cycling for CCE (b) and LHCE (c) electrolytes. (d, e) Lithium reservoir and inactive Li^0 calculated by TGC evolution over cycling for CCE (d) and LHCE (e) electrolytes.

the dense lithium reservoir is consumed, as illustrated in Supplementary Figure S2. Interestingly, the top-down images reveal that the initial porosity of the plated lithium metal at 4.3 V significantly influences the morphology of the samples discharged to 3 and 1 V. The dead lithium appears to be formed at the lithium metal grain boundaries, explaining the honeycomb-like shape observed at 3 and 1 V (marked in yellow in the top-down images in Figure 2). As a result, the smaller grain size in the CCE electrolyte, compared to LHCE, will result in higher surface area and an increased reactivity between the lithium and electrolyte. However, it is crucial to highlight the significant inhomogeneity observed in this sample, as depicted in the pictures of the copper electrode provided in Supplementary Figure S3.

As presented above, the initial irreversible capacity of the cathode results in the creation of a reservoir of active lithium at the anode. Therefore, NMC622||Cu cells cycled within the standard voltage range (4.3−3 V) will exhibit behavior similar to that of lithium metal cells. The excess lithium will compensate for the loss of lithium inventory at the anode during cycling until the reservoir is depleted. Consequently, the measured Coulombic efficiency of the cell will initially be related to the performance of the cathode.[21,22]

To confirm this, cells using CCE and LHCE electrolytes were cycled between 4.3 and 3 V at a rate of C/3-D/3; the results are presented in Figure 3a. Notably, although the first cycle of cells with the two distinct electrolytes exhibited similar behavior, those cycled with LHCE electrolytes demonstrated significantly superior cycle life compared to cells cycled with CCE. This is anticipated due to the larger lithium grain size in LHCE, resulting in reduced interfacial reactions with electrolytes. Furthermore, the reduction of LHCE electrolyte forms a salt-derived solid electrolyte interface (SEI), which has been demonstrated to be highly stable and robust against cycling.[23] Aside from cycle life, the two cycling curves exhibit a similar shape, featuring an initial plateau of retained capacity followed by a "knee", indicated in Figure 3a, and a linear decline.[12] Interestingly, this knee in the capacity retention curves aligns with a change in Coulombic efficiency when the capacity begins to decrease. Discharging the cells to 1 V after different cycle numbers reveals a distinct decrease in the voltage plateau at 1.6 V (see Figure 3b and c), with the lithium reservoir being entirely depleted after 12 and 30 cycles for CCE and LHCE, respectively. This observation validates that, in the initial plateau of retained capacity, the lithium reservoir effectively compensates for the lithium lost as inactive Li^0 or interface Li^+ at the anode. Due to the unknown impact on the cathode of the deep discharge test, cells were not subjected to further cycling after a deep discharge but were instead disassembled, and the inactive Li^0 amount was quantified by TGC (see Figure 3d and e). Surprisingly, the consumption of the lithium reservoir and the growth of inactive Li^0 both exhibit linear behavior for the two electrolytes. This observation reveals that although parasitic reactions progress more rapidly in CCE, LHCE merely slows down the process rather than stopping it. As a result, for both electrolytes the accumulated inactive Li^0 at the end of the retained capacity plateau is equal to ≈50% of the lithium reservoir initially present in those cells. These findings are in agreement with the proposed first cycle lithium inventory, suggesting that an equal amount of lithium was lost in interface parasitic reactions and in inactive Li^0 formation.

Overall, these results highlight the crucial role of the lithium reservoir in the performance of anode-free cells. By discharging

https://doi.org/10.1021/acsenergylett.4c00457
ACS Energy Lett. 2024, 9, 1693−1700

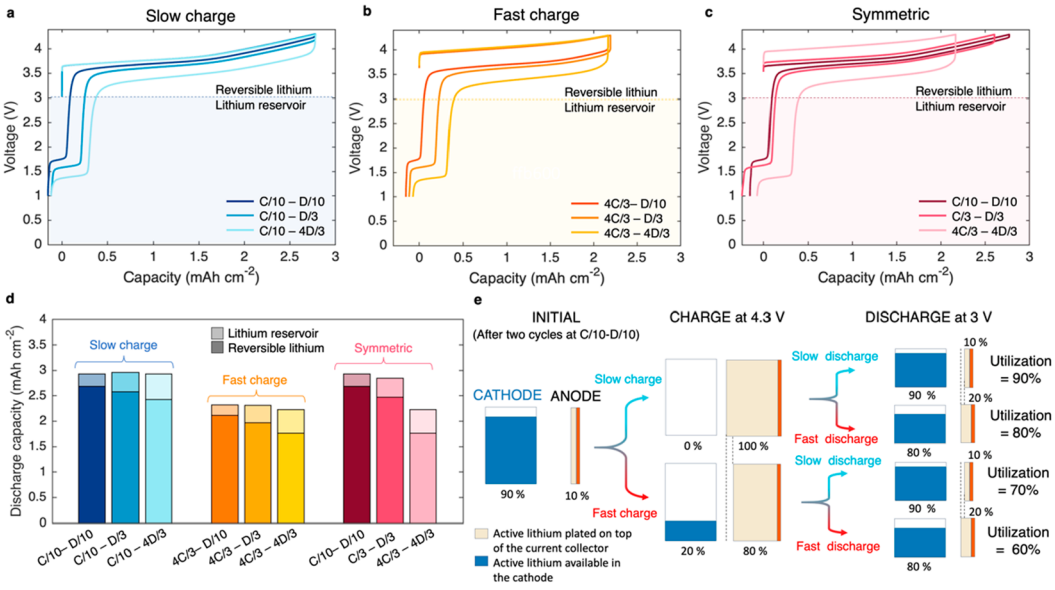

Figure 4. (a–c) Prior to applying the rate protocol, cells filled with LHCE were cycled for 2 cycles at C/10-D/10 between 4.3 and 3 V. Third-cycle charge and discharge curves between 4.3 and 1 V of cells cycled with symmetric rate (a), slow charge (b), and fast charge (c) and fully discharged to 1 V. (d) Reversible capacity and lithium reservoir capacity calculated from the discharge curve to 3 and 1 V, respectively. (e) Schematic of the lithium reservoir formation at the anode depending on the rates of charge and discharge. Percentages were calculated considering that the first charge capacity of the cell is equal to 100% of the lithium available. For clarity, lithium losses (interfaces and inactive Li^0) have been neglected in the calculation and schematic. The percentage of utilization of the lithium is calculated depending on the rate for one charge and discharge cycle between 4.3 and 3 V.

the cell to 1 V and quantifying inactive Li^0, we can accurately track the depletion of the lithium inventory. This level of precision in measurement is essential not only for comprehending the performance dynamics of anode-free cells but also to evaluate potential safety risks associated with the buildup of inactive Li^0.

Having investigated the lithium reservoir formation and evolution mechanism, our attention will now shift to its response to different C-rates. Louli et al. explored the influence of cycling conditions and demonstrated that employing an asymmetric slower charge protocol leads to reduced lithium inventory loss per cycle due to a more favorable lithium morphology.[14] Surprisingly, the impact of the current on the lithium reservoir was not explored. In the present study, three types of protocols were examined: symmetric, fast charge, and slow charge. To distinguish the initial irreversibility of the cathode and exclusively investigate the impact of the C-rate, two cycles at C/10-D/10 in the voltage range 4.3–3 V were conducted before applying the various rate protocols.

First, the anode-free cells were charged at C/10 and discharged at D/10, D/3, and 4D/3 to 1 V (Figure 4a). In this protocol, the lithium plated on the copper surface is maximized (≈2.8 mAh cm^{-2}). Notably, the reversible insertion of lithium in the cathode at 3 V depends on the discharge rate. As the current increases, the reversible capacity decreases, mainly due to charge transfer resistance, as evidenced by the large increase in the voltage curve polarization (NMC622||Cu rate tests in charge and discharge are illustrated in Supplementary Figure S4). However, the size of the plateau at 1 V suggests that the lithium that could not be reinserted back into the cathode is not lost but rather stored at the anode. In agreement, as shown in Figure 4d, the discharge capacity (from 4.3 to 1 V) is similar for the three slow charge protocols and only the ratio between the lithium that can be reversibly inserted or stored at the anode is evolving. For the cells charged at 4C/3 (see Figure 4b), the kinetic limitations of the lithium extraction from the NMC622 cathode during charging result in a smaller charging capacity (≈2.1 mAh cm^{-2}). However, with increasing discharge rates, trends comparable to those obtained with the slow charge protocol are obtained. The polarization in discharge increases with current, and the reversibility of lithium inserted within the cathode decreases while the active lithium reservoir grows. Finally, as anticipated, both the charge and discharge capacities are affected when the current is increased in charge and discharge (see Figure 4c). Increasing the current in the symmetric protocol results in a reduction of both charge and reversible capacity and an increase in the lithium reservoir at the anode.

Note that the discharge capacity is always greater than 100%, as discharging the cell to 1 V allows quantification of the combined lithium reservoir from both the initial intrinsic cathode irreversibility and polarization phenomena at high rates. The results are summarized in Figure 4d; while the charge rate impacts the amount of lithium plated on the copper current collector, the discharge rate influences the size of the remaining lithium reservoir at the anode. To understand the implications of these results on anode-free cell performance, the Figure 4e schematic illustrates the percentage of lithium utilized for each protocol along with the active lithium inventory distributed in the cathode or at the anode during charge and discharge. By adjusting the charge and discharge rates, full control over both the utilization of lithium inventory and the quantity of lithium stored in either the anode or cathode can be achieved. Consequently, in anode-free cell configurations with limited lithium, maximal utilization of the lithium occurs exclusively at low charge and discharge rates. Conversely, high charge and discharge rates result in the

https://doi.org/10.1021/acsenergylett.4c00457
ACS Energy Lett. 2024, 9, 1693–1700

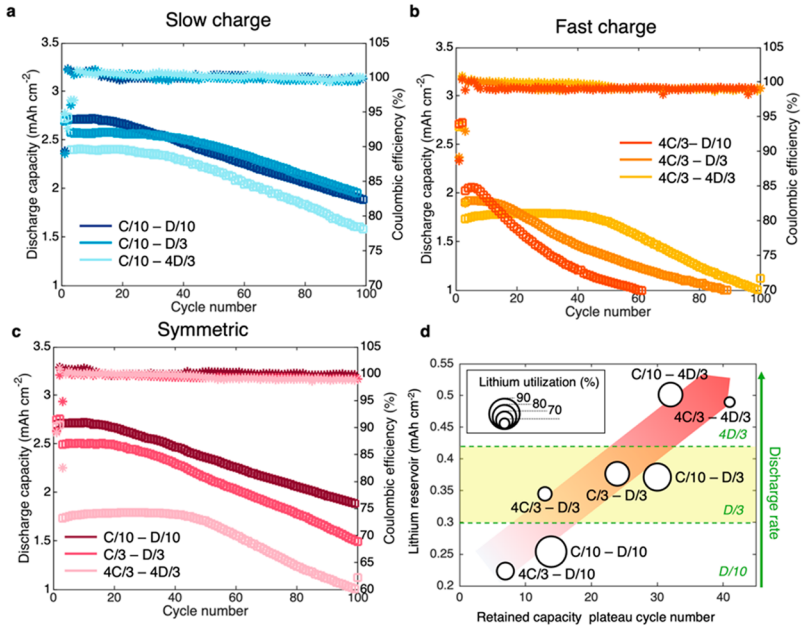

Figure 5. (a–c) Impact of C-rate and lithium reservoir on cycle life. After two cycles at C/10-D/10, anode-free cells with LHCE electrolytes were cycled using symmetric (a), slow charge (b), and fast charge (c) rate protocols between 4.3 and 3 V. (d) Lithium reservoir measured for the third cycle (summarized in Figure 4d) as a function of retained capacity plateau cycle number (the cycle number was determined using the methodology described in Supplementary Figure S7) for cells cycled with different rate protocols. The percentage of lithium utilization for each protocol is represented by circles, with larger radius indicating higher utilization.

utilization of only 60% of available lithium, with 20% remaining stored at the cathode and 20% stored at the anode.

We subsequently investigate the influence of the rate protocol and the lithium reservoir on anode-free cell long cycling. The capacity retention curves of the cells cycled with the slow charge, fast charge, and symmetric protocols are given in Figure 5a–c. In the previous section (Figure 3), we demonstrated that the initial plateau of retained capacity in the capacity over cycling number curve could be ascribed to the consumption of the lithium reservoir, thereby hindering the accurate observation of the actual degradation of the curve. Remarkably, with the different protocols, all the retention curves share a similar shape, though with a significant variation in the length of the plateau of retained capacity depending on the rate protocol. Among all of the protocols, cells cycled at C/10-D/10 (Figure 5a) and 4C/3-D/10 (Figure 5b) display the shortest plateau of retained capacity. Consistent with previous results, these two cells also have the least lithium reservoir at the anode. In contrast, cells cycled at 4C/3-4D/3 (Figure 5c) and C/10-4D/3 (Figure 5b) exhibit the longest plateau of retained capacity and possess more initial excess lithium at the anode.

The initial lithium reservoir, determined by fully discharging the cell to 1 V, was plotted against the number of cycles of the retained capacity plateau, as shown in Figure 5d. The lithium reservoir appears to correlate to the retained capacity plateau of anode-free cells, with a beneficial effect for the cells where the lithium reservoir amount is maximized. Interestingly, the mechanism described in Figure 4e holds particular significance for the long cycling of anode-free cells. The charge rate governs the total accessible active lithium inventory, while the discharge rate controls the actual ratio between the lithium utilized and the lithium reservoir. Hence, concerning enhanced lithium utilization across an extended cycle count, the protocols C/10-D/3 and C/10-4D/3 emerge as the optimal performers.

Although a correlation exists in Figure 5d between the lithium reservoir and the retained capacity plateau, it is important to note that certain protocols deviate from a perfectly linear relationship. Notably, despite having a lithium reservoir amount comparable to that of the C/10-4D/3 protocol, the cell that manifests the lengthiest plateau of retained capacity is the one undergoing cycling with the 4C/3-4D/3 protocol. Indeed, the lithium utilization of cells in these protocols will be significantly lower (60% versus 80% for the C/10-4D/3 protocol), thereby minimizing volume changes and parasitic phenomena at both the cathode and anode. Furthermore, the aggregate effect between lithium utilization, morphology, resistance growth, and the impact of storing lithium at the anode or cathode remains challenging to discriminate and is beyond the scope of this work. The impact of some of these phenomena on cell performance is summarized in Supplementary Figures S5–S7. Nevertheless, we elucidate that, among these factors, the lithium reservoir stemming solely from the cathode's limitation to de-/reintercalate the same amount of lithium at higher currents is crucial in understanding the retained capacity retention curve of anode-free cells.

In conclusion, this work provides a comprehensive understanding of the interplay between lithium utilization and reservoirs on the capacity retention and degradation behavior of anode-free cells. We demonstrated that the once-considered drawback of Ni-rich layered oxide cathodes, namely, the first cycled intrinsic irreversible capacity, can be manipulated to build a lithium reservoir at the anode and extend the cycle life of anode-free cells. However, in both CCE and LHCE electrolytes examined here, the lithium reservoir is gradually depleted due to plating/stripping irreversibility, leading to nearly 50% of the lithium lost becoming trapped as inactive Li^0,

https://doi.org/10.1021/acsenergylett.4c00457
ACS Energy Lett. 2024, 9, 1693–1700

that we quantified by TGC. This phenomenon, initially observed in the first cycle, persists over subsequent cycles, raising concerns about the actual safety of these cells. Although LHCE effectively slows down this accumulation process compared to CCE, it is essential for future electrolyte designs to specifically address this issue, concentrating on strategies to either eliminate or substantially reduce the formation of inactive Li^0.

In the second part, the formerly unclear reason for the capacity degradation discrepancy of anode-free cells under different C-rates was investigated and attributed to the correlation between lithium utilization and reservoirs. In contrast to the first-cycle irreversibility unique to the types of cathode materials, this approach can be applied to all types of cells having polarization phenomena at high currents to enhance their longevity in anode-free configurations. Consequently, by employing protocols with slow charge and fast discharge, the lithium reservoir at the anode is maximized, and the performances of the anode-free cells appear stable for a longer number of cycles. With this knowledge, one can regulate the ratio between lithium utilization and lithium reservoirs for extended capacity retention or a high initial reversible capacity designated for different applications. We believe the concept of this Li reservoir can be further extended to other approaches and opens new opportunities, taking advantage of cathode intrinsic irreversibility and kinetic limitations to extend anode-free cells' lifespan.

■ ASSOCIATED CONTENT

Supporting Information

The Supporting Information is available free of charge at https://pubs.acs.org/doi/10.1021/acsenergylett.4c00457.

Experimental procedure, comparison of first charge and discharge cycle of anode free cells with different cathodes, pictures of copper electrode after cycling, cross-section imaging of the active lithium reservoir consumption and dead lithium growth after 20 and 40 cycles, rate tests in charge and discharge, lithium reservoir and inactive Li^0 evolution at different rate protocols, and retained capacity plateau cycle number determination (PDF)

■ AUTHOR INFORMATION

Corresponding Author

Ying Shirley Meng − *Department of NanoEngineering, University of California, San Diego, La Jolla, California 92093, United States; Pritzker School of Molecular Engineering, University of Chicago, Chicago, Illinois 60637, United States;* orcid.org/0000-0001-8936-8845; Email: shirleymeng@uchicago.edu

Authors

Charlotte Gervillié-Mouravieff − *Department of NanoEngineering, University of California, San Diego, La Jolla, California 92093, United States;* orcid.org/0000-0002-4291-3428

Louis Ah − *Department of NanoEngineering, University of California, San Diego, La Jolla, California 92093, United States*

Alex Liu − *Department of NanoEngineering, University of California, San Diego, La Jolla, California 92093, United States*

Chen-Jui Huang − *Pritzker School of Molecular Engineering, University of Chicago, Chicago, Illinois 60637, United States*

Complete contact information is available at: https://pubs.acs.org/10.1021/acsenergylett.4c00457

Author Contributions

C.G., C.-J.H., and Y.S.M. conceived the original idea. C.G. developed the experimental plan with the help of C.-J.H. C.G. and L.A. conducted the experiments. A.L. and L.A. performed cryo-FIB/SEM characterization. C.G. analyzed results and prepared the manuscript with input from all authors. The final version of the manuscript was approved by all authors.

Notes

The authors declare no competing financial interest.

■ ACKNOWLEDGMENTS

The authors acknowledge Cummins Inc for funding this work. We thank Wurigumula Bao, Ruigang Zhang, and Roger Gerson for the fruitful discussions. Cryo-FIB was performed at the San Diego Nanotechnology Infrastructure (SDNI), a member of the National Nanotechnology Coordinated Infrastructure, which is supported by the National Science Foundation (Grant ECCS-1542148).

■ REFERENCES

(1) Salvatierra, R. V.; Chen, W.; Tour, J. M. What Can be Expected from "Anode-Free" Lithium Metal Batteries? *Adv. Energy Sustain. Res.* **2021**, *2*, 2000110.

(2) Yoshimatsu, I.; Hirai, T.; Yamaki, J. Lithium Electrode Morphology during Cycling in Lithium Cells. *J. Electrochem. Soc.* **1988**, *135*, 2422.

(3) Qian, J.; Adams, B. D.; Zheng, J.; Xu, W.; Henderson, W. A.; Wang, J.; Bowden, M. E.; Xu, S.; Hu, J.; Zhang, J.-G. Anode-Free Rechargeable Lithium Metal Batteries. *Adv. Funct. Mater.* **2016**, *26*, 7094−7102.

(4) Li, Q.; Cao, Z.; Liu, G.; Cheng, H.; Wu, Y.; Ming, H.; Park, G.-T.; Yin, D.; Wang, L.; Cavallo, L.; Sun, Y.-K.; Ming, J. Electrolyte Chemistry in 3D Metal Oxide Nanorod Arrays Deciphers Lithium Dendrite-Free Plating/Stripping Behaviors for High-Performance Lithium Batteries. *J. Phys. Chem. Lett.* **2021**, *12*, 4857−4866.

(5) Hu, Y.-S.; Pan, H. Solvation Structures in Electrolyte and the Interfacial Chemistry for Na-Ion Batteries. *ACS Energy Lett.* **2022**, *7*, 4501−4503.

(6) Chen, J.; Li, Z.; Sun, N.; Xu, J.; Li, Q.; Yao, X.; Ming, J.; Peng, Z. A Robust Li-Intercalated Interlayer with Strong Electron Withdrawing Ability Enables Durable and High-Rate Li Metal Anode. *ACS Energy Lett.* **2022**, *7*, 1594−1603.

(7) Ren, X.; Zou, L.; Cao, X.; Engelhard, M. H.; Liu, W.; Burton, S. D.; Lee, H.; Niu, C.; Matthews, B. E.; Zhu, Z.; Wang, C.; Arey, B. W.; Xiao, J.; Liu, J.; Zhang, J.-G.; Xu, W. Enabling High-Voltage Lithium-Metal Batteries under Practical Conditions. *Joule* **2019**, *3*, 1662−1676.

(8) Niu, C.; Liu, D.; Lochala, J. A.; Anderson, C. S.; Cao, X.; Gross, M. E.; Xu, W.; Zhang, J.-G.; Whittingham, M. S.; Xiao, J.; Liu, J. Balancing interfacial reactions to achieve long cycle life in high-energy lithium metal batteries. *Nat. Energy* **2021**, *6*, 723−732.

(9) Yu, Z.; Wang, H.; Kong, X.; Huang, W.; Tsao, Y.; Mackanic, D. G.; Wang, K.; Wang, X.; Huang, W.; Choudhury, S.; Zheng, Y.; Amanchukwu, C. V.; Hung, S. T.; Ma, Y.; Lomeli, E. G.; Qin, J.; Cui, Y.; Bao, Z. Molecular design for electrolyte solvents enabling energy-dense and long-cycling lithium metal batteries. *Nat. Energy* **2020**, *5*, 526−533.

(10) Louli, A. J.; Eldesoky, A.; Weber, R.; Genovese, M.; Coon, M.; deGooyer, J.; Deng, Z.; White, R. T.; Lee, J.; Rodgers, T.; Petibon, R.; Hy, S.; Cheng, S. J. H.; Dahn, J. R. Diagnosing and correcting anode-

free cell failure via electrolyte and morphological analysis. *Nat. Energy* **2020**, *5*, 693−702.
(11) Neudecker, B. J.; Dudney, N. J.; Bates, J. B. Lithium-Free" Thin-Film Battery with In Situ Plated Li Anode. *J. Electrochem. Soc.* **2000**, *147*, 517.
(12) Genovese, M.; Louli, A. J.; Weber, R.; Hames, S.; Dahn, J. R. Measuring the Coulombic Efficiency of Lithium Metal Cycling in Anode-Free Lithium Metal Batteries. *J. Electrochem. Soc.* **2018**, *165*, A3321.
(13) Kang, S.-H.; Yoon, W.-S.; Nam, K.-W.; Yang, X.-Q.; Abraham, D. P. Investigating the first-cycle irreversibility of lithium metal oxide cathodes for Li batteries. *J. Mater. Sci.* **2008**, *43*, 4701−4706.
(14) Louli, A. J.; Coon, M.; Genovese, M.; deGooyer, J.; Eldesoky, A.; Dahn, J. R. Optimizing Cycling Conditions for Anode-Free Lithium Metal Cells. *J. Electrochem. Soc.* **2021**, *168*, No. 020515.
(15) Zhou, H.; Xin, F.; Pei, B.; Whittingham, M. S. What Limits the Capacity of Layered Oxide Cathodes in Lithium Batteries? *ACS Energy Lett.* **2019**, *4*, 1902−1906.
(16) Lin, L.; Qin, K.; Zhang, Q.; Gu, L.; Suo, L.; Hu, Y.; Li, H.; Huang, X.; Chen, L. Li-Rich Li2[Ni0.8Co0.1Mn0.1]O2 for Anode-Free Lithium Metal Batteries. *Angew. Chem., Int. Ed.* **2021**, *60*, 8289−8296.
(17) Fang, C.; Li, J.; Zhang, M.; Zhang, Y.; Yang, F.; Lee, J. Z.; Lee, M.-H.; Alvarado, J.; Schroeder, M. A.; Yang, Y.; Lu, B.; Williams, N.; Ceja, M.; Yang, L.; Cai, M.; Gu, J.; Xu, K.; Wang, X.; Meng, Y. S. Quantifying inactive lithium in lithium metal batteries. *Nature* **2019**, *572*, 511−515.
(18) Li, M.; Wang, C.; Chen, Z.; Xu, K.; Lu, J. *New Concepts in Electrolytes. Chem. Rev.* **2020**, *120*, 6783−6819.
(19) Fang, C.; Lu, B.; Pawar, G.; Zhang, M.; Cheng, D.; Chen, S.; Ceja, M.; Doux, J.-M.; Musrock, H.; Cai, M.; Liaw, B.; Meng, Y. S. Pressure-tailored lithium deposition and dissolution in lithium metal batteries. *Nat. Energy* **2021**, *6*, 987−994.
(20) Chen, S.; Zheng, J.; Mei, D.; Han, K. S.; Engelhard, M. H.; Zhao, W.; Xu, W.; Liu, J.; Zhang, J.-G. High-Voltage Lithium-Metal Batteries Enabled by Localized High-Concentration Electrolytes. *Adv. Mater.* **2018**, *30*, 1706102.
(21) Adams, B. D.; Zheng, J.; Ren, X.; Xu, W.; Zhang, J.-G. Accurate Determination of Coulombic Efficiency for Lithium Metal Anodes and Lithium Metal Batteries. *Adv. Energy Mater.* **2018**, *8*, 1702097.
(22) Huang, C.-J.; Thirumalraj, B.; Tao, H.-C.; Shitaw, K. N.; Sutiono, H.; Hagos, T. T.; Beyene, T. T.; Kuo, L.-M.; Wang, C.-C.; Wu, S.-H.; Su, W.-N.; Hwang, B. J. Decoupling the origins of irreversible coulombic efficiency in anode-free lithium metal batteries. *Nat. Commun.* **2021**, *12*, 1452.
(23) Cao, X.; Jia, H.; Xu, W.; Zhang, J.-G. Review—Localized High-Concentration Electrolytes for Lithium Batteries. *J. Electrochem. Soc.* **2021**, *168*, No. 010522.

https://doi.org/10.1021/acsenergylett.4c00457
ACS Energy Lett. 2024, 9, 1693−1700